How to cite: *Angew. Chem. Int. Ed.* **2020**, *59*, 17145 – 17153
International Edition: doi.org/10.1002/anie.202001816
German Edition: doi.org/10.1002/ange.202001816

Lithium Metal Batteries

Wetting Phenomena and their Effect on the Electrochemical Performance of Surface-Tailored Lithium Metal Electrodes in Contact with Cross-linked Polymeric Electrolytes

Mengyi Zhang, Jens Becking, Marian Cristian Stan, Arthur Lenoch, Peter Bieker, Martin Kolek, and Martin Winter**

Abstract: *Li metal batteries (LMBs) containing cross-linked polymer electrolytes (PEs) are auspicious candidates for next-generation batteries. However, the wetting behavior of PEs on uneven Li metal surfaces has been neglected in most studies. Herein, it is shown that microscale defect sites with curved edges play an important role in a wettability-dependent electrodeposition. The wettability and the viscoelastic properties of PEs are correlated, and the impact of wettability on the nucleation and diffusion near the Li | PE interface is distinguished. It is found that the curvature of the edges is a key factor for the investigation of wetting phenomena. The appearance of microscale defects and phase separation are identified as main causes for erratic nucleation. It is emphasized that the implementation of stable and consistent long-term cycling performance of LMBs using PEs requires a deeper understanding of the "soft-solid"–solid contact between PEs and inherently rough Li metal surfaces.*

Introduction

Li metal batteries (LMBs) have attracted renewed attention as one of the promising evolutionary battery systems that could allow higher energy densities than state-of-the-art Li ion batteries (LIBs) by taking advantage of the high specific capacity (3860 $mA\,h\,g^{-1}$) and low standard potential (−3.040 V vs. standard hydrogen electrode) of the Li metal electrode.[1–5] In spite of that, Li metal electrodes have a high chemical reactivity which leads to (spontaneous) formation of surface layers and nontrivial interphases.[6–8] During electrodeposition/electrodissolution, such interphases and surface topographies are further altered and partially rebuilt, resulting in complex and dynamic surface conditions.[9–12] Li electrodeposition is also accompanied by the formation of so-called high-surface-area Li (HSAL) which in turn is being formed as a result of uncontrolled accumulation of Li deposits.[13,14] Safety concerns regarding such hazardous HSAL formation and a possible cascade of unwanted reactions with flammable electrolyte components are presumed.[15,16] One approach to develop safe LMBs is the use of electrolytes which do not tend to decompose or at least show a high hindrance towards decomposition when in contact with the Li metal surface.[17] Besides that, these safe electrolytes should feature a high elastic modulus and uniform adhesion to accommodate volumetric changes of the Li metal electrodes during cycling.[5,18,19] The typical examples are solid electrolytes (SEs) primarily based on polymers, glasses, and/or ceramics.[20–22] Aside from inorganic electrolytes, the approaches based on polymers, known as solid polymer electrolytes (SPEs), have attracted increased interest as they offer several advantages.[19,23] Especially their high degree of flexibility is assumed to withstand the volume change of Li metal electrodes during the electrodeposition/electrodissolution process.[24,25] As an important example, the incorporation of a Li salt into a UV-cross-linked poly(ethylene oxide) (PEO) matrix hinders the crystallization of PEO at room temperature and results in an elastic SPE.[26] Further on, it was reported that PEs after UV-induced cross-linking are self-standing with good thickness and shape retention which renders such systems promising candidates to offset morphological transformations.[27] Cross-linked ternary solid polymer electrolytes (TSPEs) based on this approach, together with the plasticizing effect of an ionic liquid (IL), show a next development stage towards highly amorphous PEs with improved ionic conductivity.[26,28]

Aside from electrolyte development, Li | electrolyte interfacial/interphasial properties are the key fundamentals for LMB research.[8,34] One essential concept to understand the Li | electrolyte interfacial/interphasial behaviors is the solid electrolyte interphase (SEI) model, in which the Li metal surface is mainly idealized as a flat plain consisting of natural surface species, for example, Li_2CO_3 and Li_2O.[6,12,35] However, it should be stressed that the topographic inhomoge-

[*] M. Zhang, J. Becking, Dr. M. C. Stan, Dr. P. Bieker, M. Kolek, Prof. M. Winter
MEET Battery Research Center
Institute of Physical Chemistry, University of Münster
Corrensstraße 46, 48149 Münster (Germany)
E-mail: martin.kolek@uni-muenster.de
martin.winter@uni-muenster.de
A. Lenoch, Dr. P. Bieker
Institute of Physical Chemistry, University of Münster
Corrensstraße 28/30, 48149 Münster (Germany)
Prof. M. Winter
Helmholtz Institute Münster, IEK-12
Forschungszentrum Jülich GmbH
Corrensstraße 46, 48149 Münster (Germany)
E-mail: m.winter@fz-juelich.de
Supporting information and the ORCID identification number(s) for the author(s) of this article can be found under: https://doi.org/10.1002/anie.202001816.

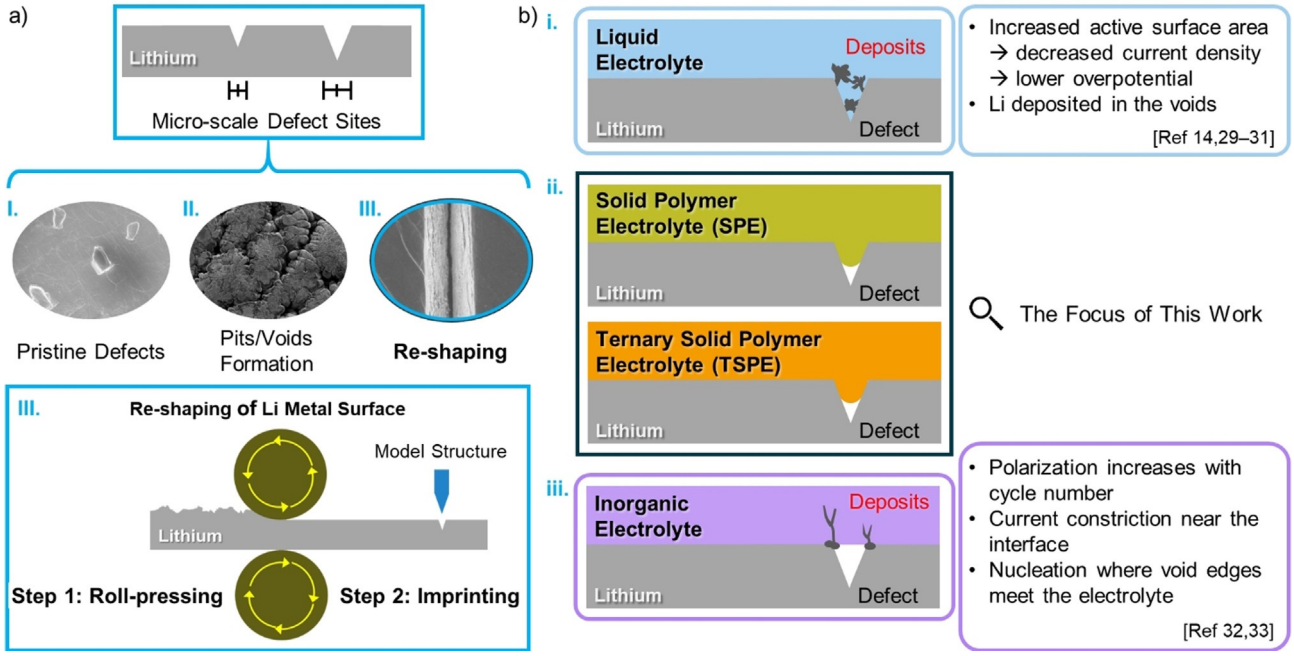

Figure 1. Research scope of this work: a) Microscale defect sites resulting from I. pristine defects during production process, II. pits/voids formation during Li electrodeposition/electrodissolution, and III. mechanical modification. The Li metal surfaces with V-shaped defects presented herein are prepared by a so-called "reshaping" process which includes the roll-pressing of the pristine Li metal foils and the intentional reshaping with model structures. b) The effect of microsized defects on the wetting and electrochemical performances of Li metal electrodes: i. with liquid electrolytes reported in refs. [14, 29–31]; ii. with **SPE**/**TSPE** in this work; iii. with an inorganic electrolyte reported in refs. [32, 33].

neity of the uneven Li metal surface with microscale defect sites under practical conditions is a mostly neglected interfacial and interphasial property.[7,14,32,36,37] An overview of the origins of microscale defect sites on Li metal electrodes is displayed in Figure 1 a.

Pristine Li foils exhibit native surface roughness respectively pristine defects at microscale which are mainly generated during production (Figure 1 a.I).[38] Furthermore, formation of pits/voids can be observed during cycling (Figure 1 a.II),[33,39,40] whereas intentionally introduced mechanical modifications (e.g. roll-pressing, needle or block treatment, Figure 1 a.III)[14,30,31,38] of the Li metal surface can be used to engineer and to study the Li | electrolyte interface, as well the interphases. Herein, we use the term "reshaping" for the mechanical modifications of previously smoothened (e.g. via the roll-pressing method[38]) Li metal surfaces.

The wetting phenomena of Li metal surfaces by electrolytes become crucial when microsized defect sites are present. While liquid electrolytes mostly show a complete wetting of rough Li metal surfaces, SEs face an underlying challenge to achieve homogeneous and intimate solid–solid contacts.[41,42] The Li | inorganic electrolyte interface reveals certain issues, and also polymer-based electrolytes show limitations, with wetting microscale defects on the Li metal surface.[43] In literature, the effects of such defect sites on the Li electrodeposition have been reported for liquid and inorganic electrolytes (Figure 1 b).[14,29–33] In the case of liquid electrolytes (Figure 1 b.i), due to a much better wetting of the Li metal surface, microscale defect sites lead to increased active surface area and decreased effective current density, resulting in lower overpotentials for electrodeposition.[14,29–31] Moreover, after electrodissolution, the electrochemically induced microscale pits tend to be "hot spots" for Li nucleation and deposition.[29] At the interface between inorganic electrolytes and Li (Figure 1 b.iii), poor wetting in accordance with polarization and Li nucleation at void edges was observed.[32] As an example for inorganic electrolytes, Krauskopf et al. reported current constriction phenomena at $Li_{6.25}Al_{0.25}La_3Zr_2O_{12}$-based SEs near the interface where small contact spots were present.[33] Detailed studies on the influence of microscale defects on the wetting behavior of PEs and its effect on the electrochemical behavior, however, are rarely reported.

In this work, we shed light on the wetting phenomena (Figure 1 b.ii) of a PEO-based cross-linked SPE (LiTFSI-PEO, in the following referred to as **SPE**) and a TSPE (LiTFSI-PEO-Pyr_{14}TFSI, referred to as **TSPE**) in combination with a reshaped Li metal electrode. Microsized defect sites, referred further to as V-shaped imprints, were artificially created in order to mimic the wetting of uneven Li metal surfaces by the PEs. The wettability and related viscoelastic properties of **SPE** and **TSPE** are compared and the impact of wettability on the electrochemical performance is distinguished.

Results and Discussion

A roll-pressed Li metal electrode is used as a benchmark to approach an ideally flat surface.[38] The V-shaped imprints (reshaping, Figure 1 a.III) were created using an in-house developed tool to decorate the surface of roll-pressed Li

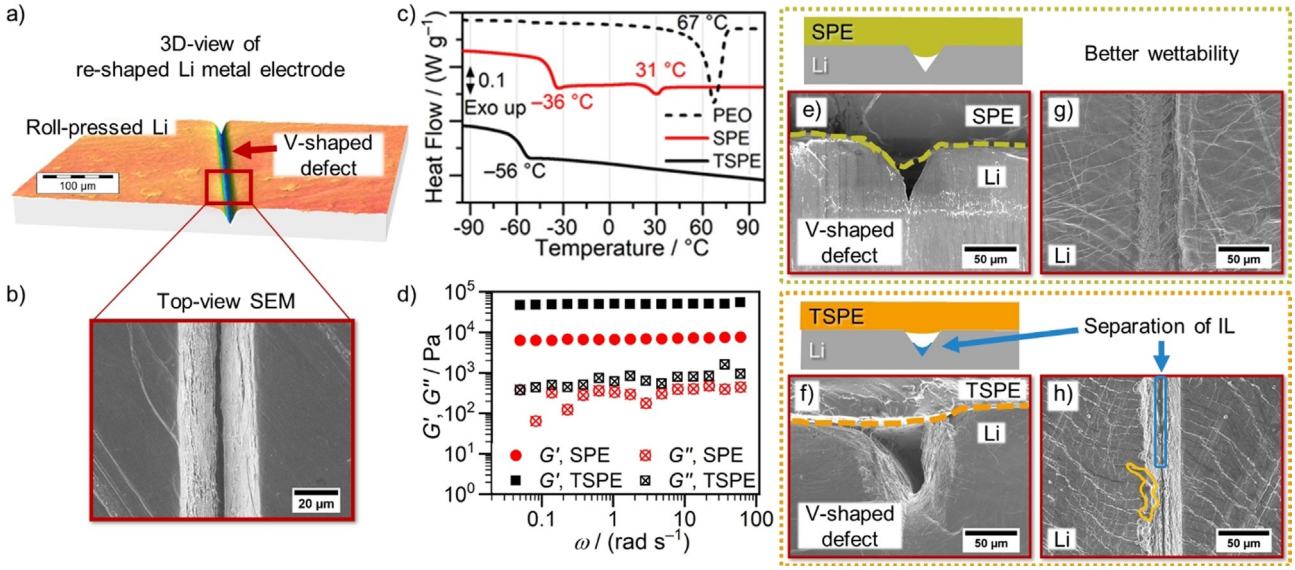

Figure 2. Wetting behaviors of **SPE** and **TSPE** on reshaped Li metal electrodes: a) 3D laser scanning microscope image (20× magnification) and b) top-view SEM image of the V-shaped Li metal electrode. c) Differential scanning calorimetry (DSC) heating traces of PEO, **SPE**, and **TSPE** membranes with a rate of 10 K min^{-1}. d) Dynamic moduli G', G'' for **SPE** and **TSPE** membranes as a function of angular frequency ω measured by oscillatory rheology at 60 °C. Cross-sectional SEM images of the V-shaped Li metal electrode wetted by e) **SPE** and f) **TSPE**. Top-view SEM images of Li metal surfaces after 24 h storage at 60 °C using a g) **SPE** and h) **TSPE** membrane. In (f) orange areas denote **TSPE** residues after detachment, blue areas denotes an IL-rich phase characterized by EDS (Figure S2 and Table S1).

metal electrodes. An adjustable blade in depth resulted in a broadening of V-shaped imprints with curved edges. Topographic investigations carried out by means of 3D laser scanning microscopy of the reshaped Li metal surface (Figure 2a) revealed the successful application of V-shaped defects without affecting the surrounding area on the roll-pressed electrode nearby. The top-view SEM image of a V-shaped defect presented in Figure 2b shows smooth, curved edges of the imprint at the Li metal surface.

Viscoelasticity-Dependent Wettability

The interfacial properties of **SPE** and **TSPE** with the Li metal surface, implying their wetting behavior, strongly depend on the thermal and viscoelastic properties of such cross-linked PEs. Figure 2c shows DSC results of heating scans of **SPE** and **TSPE** between −90 °C and 100 °C. The thermogram of **SPE** (red curve) displays a glass transition at −36 °C and a melting peak at 31 °C, presenting the existence of an amorphous phase at 60 °C. The decreased melting temperature of the **SPE** compared to PEO (67 °C, dashed black curve) can be attributed to the cross-linking process which facilitates the amorphization of PEO in the presence of LiTFSI.[27] The presence of the IL ($Pyr_{14}TFSI$) in the cross-linked **TSPE** system changes the observed glass transition to −56 °C (black curve), without a distinct melting step during the heating scan. Based on the results, it can be concluded that **TSPE** maintains its amorphous behavior over a wide temperature range. As reported in previous studies, cross-linked PEO-based membranes can be characterized as rubber-like or "soft-solid" and show elastomeric behavior.[39,44,45] Mechanical properties are important to further understand the interplay between PE membranes and Li metal electrodes in electrochemical cells. In general, the physics underlying "soft solid"–solid wetting, as in Li | PEs, can be understood by mechanical deformation processes, governed by the viscoelastic properties of the PE. The viscoelastic behavior of **SPE** and **TSPE** was quantified by oscillatory rheological measurements and the results are presented in Figure 2d and Figure S1a. The frequency response of the storage modulus (G') and loss modulus (G''), representing elastic and viscous contributions, respectively, is presented in Figure 2d. Within the observed range, G' and G'' values of **SPE** and **TSPE** show a frequency-independent behavior, which is typical for strongly cross-linked gels.[46] As G' exceeds G'' for at least an order of magnitude, **SPE** and **TSPE** both remain predominantly elastic over the complete frequency range. The higher magnitude of G' values of **TSPE** compared to **SPE** is associated with higher mechanical rigidity and a more solid-like character of the **TSPE** membrane.[46] Considering the higher damping factor (tanδ) for **SPE** (Figure S1a), mechanical stresses are more easily dissipated in the **SPE**, thus, an easier adaption to morphological changes, like the presence of defects on Li metal surfaces, can be anticipated.

From cross-sectional SEM images (Figure 2e,f), it is found that the **SPE** is able to "flow" into the V-shaped defect after 24 hours while the **TSPE** tends to retain its original shape and, therefore, shows less wetting. This was confirmed by PE "infiltration" experiments (Figure S1b,c) into a glass microfiber filter at 60 °C. In other words, the poorer wetting behavior of the **TSPE** can be related to its more solid-like viscoelastic properties, as discussed for the oscillatory rheological measurements. Figure 2g and 2h show top-view SEM images of reshaped Li metal electrodes after removal of the respective electrolyte. The electrodes were stored at 60 °C for

24 hours. A homogeneous defect structure can be observed at the surface of the V-shaped Li metal electrode aged with **SPE**, while for **TSPE**, residues were observed within the V-shaped defect. Using EDS investigations of the residues present in the **TSPE** (Figure S2, Table S1), the presence of an IL phase at the bottom of the V-shaped defect (Figure 2h, blue area) was identified. Meanwhile, membrane-derived species (Figure 2h, orange area) were found at the wall of the defect. Such phase separation phenomenon is assumed to be related to the elastic properties of the **TSPE** which do not allow the membrane to deform at small scales thus leading to a "squeezing" effect of the IL at 60 °C.

The strongly varying wetting behavior of **SPE** and **TSPE** is expected to have an influence on the electrochemical performance of V-shaped Li metal electrodes as well. The effect of wettability on the electrochemical characteristics of battery cells are widely discussed for liquid electrolyte systems with separators.[47] However, our findings reveal that the difference of wettability in case of cross-linked PEs, which is rarely discussed in literature, could be also regarded as key parameter to explain the overpotential evolution during cycling in Li | PE | Li cells. As shown in Figure S3 a,b, a lower and relatively stable voltage is observed during electrodeposition/electrodissolution in a symmetrical Li | **SPE** | Li cell compared to Li | **TSPE** | Li using as-received Li metal electrodes. This stands in contrast to the impedance data obtained by electrochemical impedance spectroscopy (EIS) presented in Figure S3 c,d where higher resistance values (i.e. R: Ohmic series resistance, R_{ct}: charge transfer resistance, and R_{pas}: passivation layer resistance) for Li | **SPE** | Li compared to Li | **TSPE** | Li cells are observed. Based on these results, a higher effective contact area of the electrochemical interface/interphase for the Li | **SPE** | Li cells is assumed. This could be further explained by a better wettability on V-shaped Li metal electrodes by **SPE** at 60 °C compared to **TSPE**. As reported by Inada et al., a positive correlation between enhanced wettability and improved cycling stability was also observed at the interface between Li metal electrodes and garnet-type SE pellets by preheating at 175 °C (5 °C lower than the Li metal melting point) before cycling at room temperature.[48]

Local Wettability Derived Li Nucleation

For a deeper understanding on the impact of the wettability at the Li | PE interfaces, the Li nucleation behavior in dependence of locally varied wettability was investigated in both systems. The influence of the V-shaped morphology on the inherent correlation between wettability and Li nucleation was analyzed at the initial stage with an areal electrodeposition capacity of 0.1 mAh cm^{-2} and a current density of 0.1 mA cm^{-2}. It needs to be mentioned that the determination of the nucleation stage based on the voltage spike observed at the onset of Li electrodeposition was not considered in this case. Therefore, the nucleation stage is defined herein as the period before the plateau overpotential occurs (here at 0.1 mAh cm^{-2}).[5,49–51] The reshaping of the Li surface is discussed in detail in the Supporting Information (Figures S4–S8). We employed two different imprint depths (d), which generate asymmetric "sharp" (high curvature, $\approx(9\,\mu m)^{-1}$) and "smooth" edges (low curvature, $\approx(14\,\mu m)^{-1}$) in shallow imprints ($d\approx20\,\mu m$), as well as symmetric "smooth" edges (low curvature, $\approx(15\,\mu m)^{-1}$) in deeper imprints ($d\approx30\,\mu m$), as illustrated in Figure 3a. Additionally, roll-pressed Li was used as a zero-curvature reference.[38]

On the Li metal surface with the shallow imprint (Figure 3 b,d, **SPE** and **TSPE**, respectively), after electrodeposition at 0.1 mA cm^{-2}, the preferential Li nucleation sites are located on the sharp edge of the V-shaped Li electrode with higher curvature, whereas for the deeper imprint (Figure 3 c,e, **SPE** and **TSPE**, respectively), Li deposit growth occurs in a horizontal direction and the Li deposits are accumulated tending to fill the defect (for higher electrodeposition capacity see Figure S9).

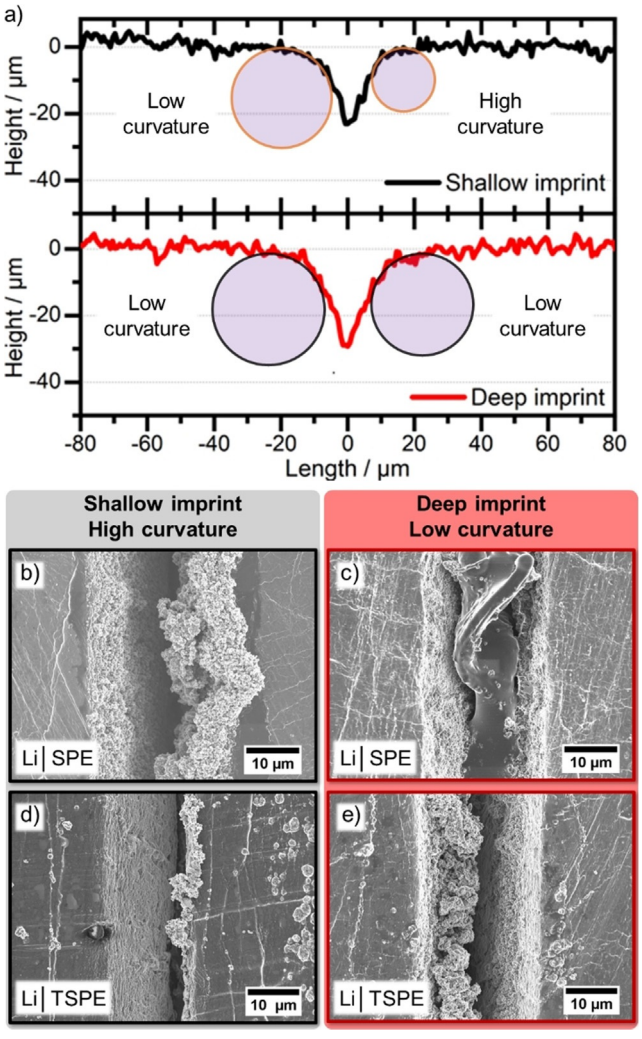

Figure 3. Effect of V-shaped defects on Li nucleation sites after initial electrodeposition: a) Height profile of shallow imprint and deep imprint, the curvatures of the edge are defined as osculating circles. For more details please see Figure S8. SEM images of Li metal electrodes after 1 h electrodeposition with 0.1 mA cm^{-2}: b) with shallow imprint using **SPE**; c) with deep imprint using **SPE**; d) with shallow imprint using **TSPE**; e) with deep imprint using **TSPE**.

The V-shape-induced physical contact and wettability between the polymer electrolytes and Li metal electrodes can be used to rationalize the observed nucleation behavior:

1) High curvatures can improve localized contact between PEs and the Li metal surface where tip-induced nucleation is favored and charges accumulate along the edged shape.[43,49,52]
2) Low curvatures can improve the overall wettability between PEs and defect surfaces rather independent of the elastomeric properties of **SPE** and **TSPE**.
3) A competitive Li nucleation behavior between the defect and the roll-pressed surface in the surrounding is observed in Figure 3b–e. At the reshaped Li | **SPE** interface, Li predominately nucleates in the microscale defects regardless of the morphologies of the V-shaped imprint. However, at the reshaped Li | **TSPE** interface with high curvature, significant Li nucleation sites are found on the roll-pressed surface although the curvature of edges can tailor competitive trends (Figure 3d).

The 3D surface representation of the roll-pressed region shown in Figure 2a reveals that defects (at a scale of few micrometers) are still visible after surface homogenization.[38] Such defects can act as additional nucleation sites if the intimate contact (wetting) to the roll-pressed Li is not ensured. The differences between the wetting behavior of the **SPE** and **TSPE** membranes with Li metal electrodes are further investigated for "zero-curvature only" roll-pressed Li metal electrodes where no V-shaped defects were present. On the roll-pressed Li metal electrodes, inhomogeneous and larger nuclei in Li | **TSPE** | Li (0.1 mA cm^{-2}, 1 h) are formed with sizes ranging from ≈0.5 μm up to ≈7.0 μm, as shown in Figure S10a. The Li nuclei size in Li | **TSPE** | Li was further investigated with the same deposition areal capacity but at 0.01 mA cm^{-2} (Figure S10b) and resulted in smaller nuclei sizes compared to the ones occurring at 0.1 mA cm^{-2}. In Li | **SPE** | Li cells at 0.1 mA cm^{-2}, small Li nuclei (≈1 μm) are distributed homogenously on the Li metal surface (Figure S10c). These results indicate that the **TSPE** suffers from inhomogeneous surface contact resulting in lower effective contact areas (A_{eff}) due to relatively poor wettability on intrinsic surface defects after roll-pressing.

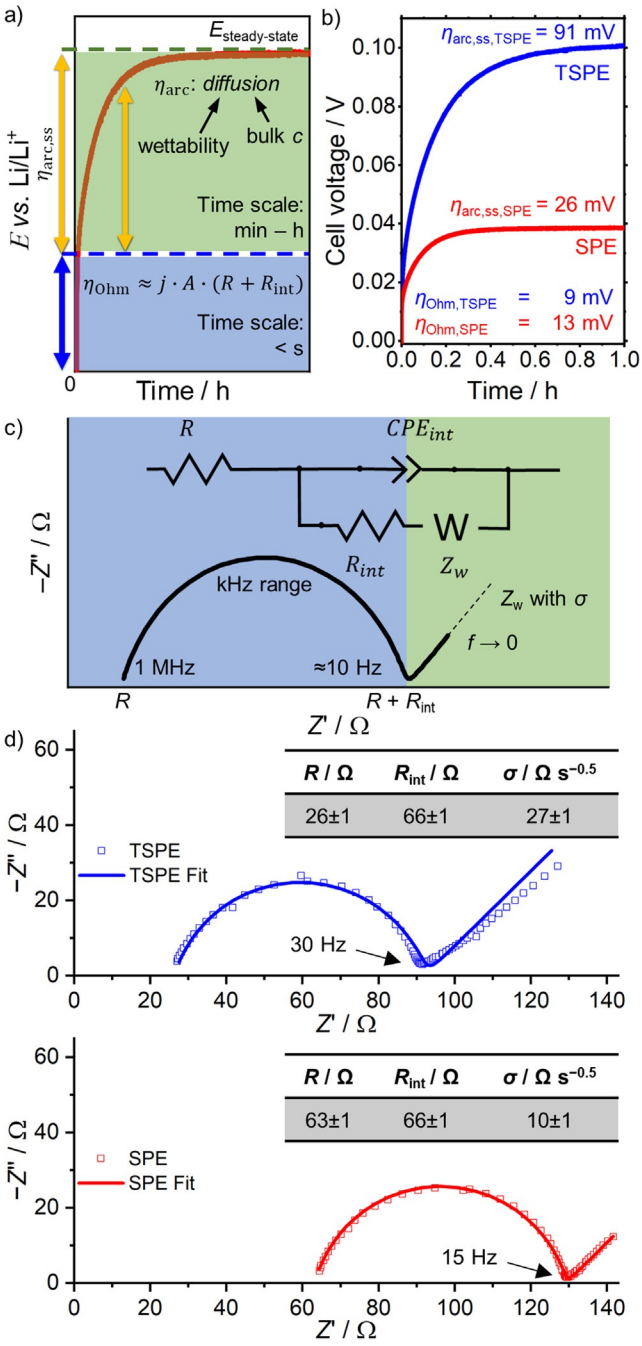

Figure 4. a) Illustration of a representative cell potential *E* profile, a potential drop following Ohm's law (η_{Ohm}), and an overpotential as an arc shape (η_{arc}) before it reaches a steady-state potential ($\eta_{arc,ss}$). The applied current density should ensure ion depletion-free interfaces and therefore it should be in the range of the exchange current density value for the system (here: ≈0.1 mA cm^{-2}).[28] b) Representative time-dependent cell voltage *E* response of Li | **SPE** | Li and Li | **TSPE** | Li using roll-pressed Li metal electrodes with 0.1 mA cm^{-2} indicating overpotential contributions. c) An exemplary Nyquist plot and the equivalent circuit model used for impedance measurements showing different contributions based on their frequency range. d) Obtained EIS data and corresponding fitting results of Li | **TSPE** | Li and Li | **SPE** | Li cells at 60 °C.

Wettability-Dependent Electrochemical Interfaces

As a next step, the cell voltage (E) response of Li metal electrodes during electrodeposition was correlated with the wettability properties of the PEs. We describe this response based on wettability-dependent electrochemical interfaces in PE-based LMBs. Following Figure 4a, the response of E to a moderate constant current density (≈0.1 mA cm^{-2} for the observed systems) consists of a potential drop deducing Ohm's law (η_{Ohm}) (Figure S11) and an arc-shaped overpotential response (η_{arc}) before reaching a steady-state potential ($E_{steady\text{-}state}$).[53,54] When a constant current density j is applied, η_{Ohm} evolves immediately at a very short time scale (≪ seconds), while η_{arc} arises within seconds and minutes, and $E_{steady\text{-}state}$ is typically reached within minutes or sometimes hours (strongly depending on the observed system).[51] The translation of the theoretical $E(t)$ response to the

observed data for Li | PE | Li cells is depicted in Figure 4b and displays a similar shape with a roughly three times lower η_{arc} for **SPE**-based cells ($\approx$26 mV) compared to **TSPE**-based cells ($\approx$91 mV). Interestingly, η_{Ohm} shows the opposite trend and is slightly higher for the **SPE**-based cell ($\eta_{Ohm,SPE} \approx 13$ mV; $\eta_{Ohm,TSPE} \approx 9$ mV). Figure 4c presents a typical Nyquist plot and an equivalent circuit model used for fitting of the data. The constant phase element (CPE)-modified Randles circuit comprises the Ohmic resistance R, the interfacial/interphasial resistance R_{int} (including R_{ct} and R_{pas}), and the Warburg element (Z_W). Depending on the frequency of the voltage perturbation, R is found at the high-frequency region ($\gg$kHz) of EIS while R_{int} is obtained at a high to intermediate frequency range (kHz–Hz). The R and R_{int} values can be correlated with η_{Ohm} using the equation $\eta_{Ohm} \approx jA\ (R + R_{int})$. η_{arc}, however, comprises significant influences by the diffusion properties of the systems (Figure S11). By analysis of the Warburg impedance (Z_W) in EIS at low frequencies (<10 Hz), additional information about mass transport properties can be derived.[55,56] As illustrated in Figure 4d, the low-frequency region (<10 Hz) reveals a distinct diffusion contribution with a phase angle of $-\pi/4$ (45° slope) which indicates that solid-state diffusion processes play a crucial role for understanding the ongoing complex electrochemical behaviors at the Li | PE interface.[57,58] In this work, we assume the Warburg impedance to follow a semi-infinite linear diffusion model.[57] It can be expressed by $Z_W = \sigma(i\omega)^{-0.5} = \sigma\omega^{-0.5}(1-i)/\sqrt{2}$, where σ is the Warburg coefficient [$\Omega\,s^{-0.5}$], ω is the frequency, and i is the imaginary unit.[57] The Warburg coefficient σ can be regarded as a diffusion-associated resistance, and it was reported by Huang et al. that higher Warburg coefficients were found to be the main reason for high polarization losses of $YBa_2Cu_3O_{7-\delta}$ | PAN-based electrolyte | Li solid-state batteries.[59]

The results presented in Figure 4d therefore reveal varying diffusion contributions for Li | **TSPE** | Li and Li | **SPE** | Li cells. The "ideal" ($\approx$45°) Warburg diffusion part for the Li | **SPE** | Li cells with a σ value of 10 $\Omega\,s^{-0.5}$ stands in contrast to the $<45°$ diffusion region of the **TSPE**-based system with a higher σ of 27 $\Omega\,s^{-0,5}$. Even though the Li | **TSPE** | Li cell shows lower $R + R_{int}$ values and similar R_{int} values compared to Li | **SPE** | Li, the higher η_{arc}, as observed in Figure 4b, can be rationalized by the almost three times higher σ. It is emphasized that the intuitive interpretation of the $E(t)-(R+R_{int})$ correlation is not valid for the observed systems where PEs are employed. The interpretation, based on liquid electrolyte systems, considers the presence of a fully wetted interface/interphase and fast Li ion migration/diffusion processes in the bulk electrolyte.[9] This rapid and non-tortuous Li ion transport through the interphases results in a negligible contribution of wettability-dependent mass transport to the polarization of the Li electrodeposition/electrodissolution processes.[60] However, this understanding of the Li | liquid electrolyte interface without considering diffusion processes and the influence of wettability on rough surfaces, fails to explain the coexistence of the high interfacial/interphasial resistance and low E, as well as Z_w, as observed within this work for Li | PE interfaces. We therefore suggest a wettability-dependent electrochemical interface which takes in consideration the wettability properties of the PEs and the shape of the Li metal surface as indicated in Figure S12.

The measured Warburg coefficients of cells with different Li metal surface topographies listed in Table S2 demonstrate that for Li | **SPE** | Li cells no clear relationship of curvature and σ can be found (10–15 $\Omega\,s^{-0.5}$). In contrast, σ of Li | **TSPE** | Li cells with low-curvature V-shaped electrodes result in a decreased value of 13–18 $\Omega\,s^{-0.5}$ compared to 25–30 $\Omega\,s^{-0.5}$ for high-curvature and roll-pressed electrodes. This observation further supports the pronounced wettability-dependent nature of **TSPE** by consideration of the complex interface, including IL phase separation and the viscoelastic properties. Additionally, a decreased σ value (Figure S13) is also observed after preheating at 90 °C of Li | **TSPE** | Li cells, indicating beneficial diffusion conditions (while R_{int} is increased, but the overvoltage is reduced).

The corresponding overvoltage curves for symmetric Li | PE | Li cells with V-shaped Li metal electrodes are presented in Figure 5a–d. Similar to the conclusions drawn from the impedance data, the steady-state $\eta_{arc,ss}$ values of Li | **SPE** | Li cells ($\approx$20 mV) are stable for each Li surface topography (Figure 5a) as well as during cycling (Figure 5c). For Li | **TSPE** | Li, however, $\eta_{arc,ss}$ varies rather strongly between 40 and 70 mV (Figure 5b) and is therefore sensitive to the change of curvature. The lowest $\eta_{arc,ss}$ can be observed at low-curvature while the values increase for zero-curvature and especially for high-curvature reshaping. The $\eta_{arc,ss}$ values during cycling, however, only differ slightly. The low-curvature defects with broader edges are beneficial for the low-plasticity **TSPE** combined with separation of IL which can be seen in Figure S14 as well, where the presence of lower-curvature defects elongates the cycling stability of Li | **TSPE** | Li cells. This might be correlated with established ionic pathways between the **TSPE** membranes and IL in the V-shaped defects. The **SPE** reveals a more stable wettability-dependent electrochemical interface which can be correlated with the viscoelastic properties and homogeneous diffusion conditions.

The importance of these findings is further illustrated for LFP | PE | Li full cells. The potential profiles of the cathode (LFP; WE) and anode (Li; CE) are presented in Figure S15. The same trend as for the E response discussion can be seen here as well.

Depending on the type of curvature, the overpotentials of the reshaped electrodes differ, with being the most beneficial for low curvature Li samples. Besides the intrinsic differences of cathode wetting by **SPE** and **TSPE**, which results in better capacity utilization for the **TSPE** (likely because of the IL phase[61]), the overpotentials of the Li anode are lower for the **SPE** compared to the **TSPE**. The wettability-dependent electrochemical interface can be therefore considered as an important factor for the determination of interfacial properties of PE-based LMBs.

It is further emphasized that the revealed squeezing effect of the IL, which contains Li salt, from the **TSPE** into the bottom of the V-shaped defect sites could facilitate Li nucleation and Li growth on the surface inside the defects

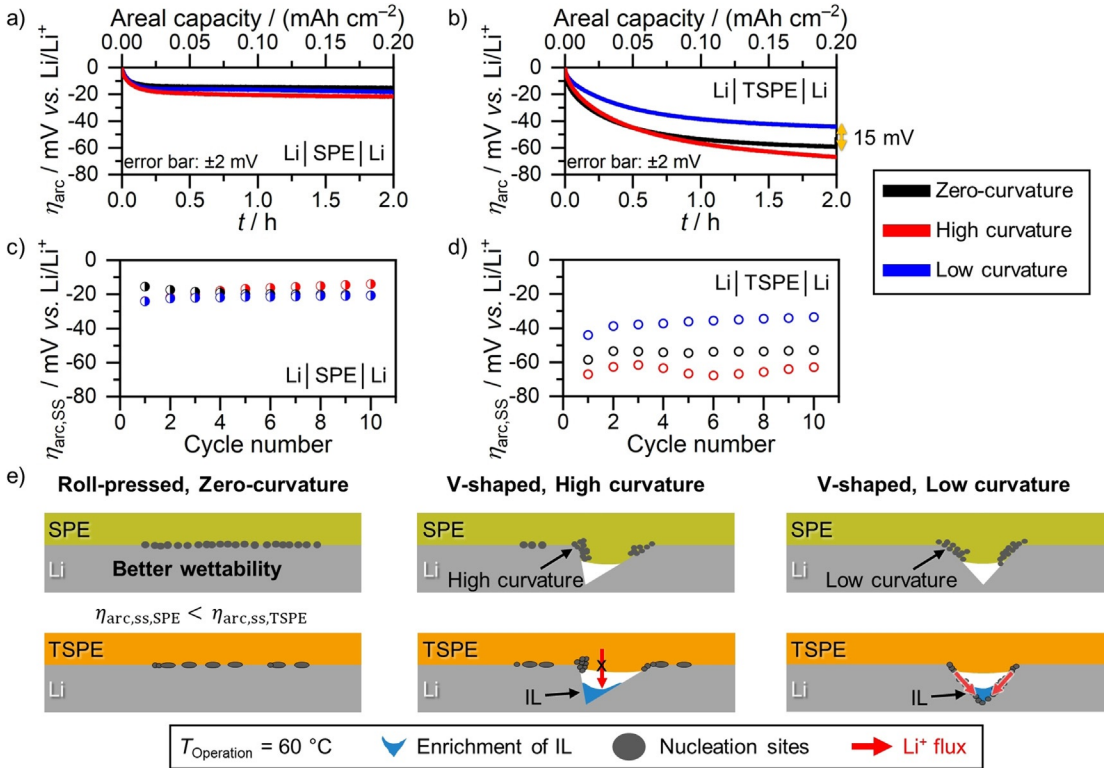

Figure 5. Correlation of Li surface topographies (zero-curvature/roll-pressed, high-curvature, and low-curvature) and overpotentials η_{arc} during electrodeposition (0.1 mA cm^{-2}, 0.2 mAh cm^{-2}) in a,c) Li | **SPE** | Li and b,d) Li | **TSPE** | Li cells recorded in three-electrode configuration. a,b) Potential vs. time plot of the η_{arc} response at the first cycle; c,d) Evolution of steady-state overpotential $\eta_{arc,ss}$ of the Li metal electrodes with cycle number in c) Li | **SPE** | Li and e) Li | **TSPE** | Li cells recorded in three-electrode configuration. e) Illustration of the effect of wetting behaviors on the electrochemical performance of Li electrodeposition summarizing the wettability, EIS, and *E* response.

in Li | **TSPE** | Li cells, if physical contact between the bulk electrolyte and the IL phase is kept intact (Figure S16). This could lead to defect wettability where Li deposits can grow inside the voids and could lead to reduction of vertical Li growth and, therefore, prevention of penetration of PEs. Besides TSPEs, gel polymer electrolytes (GPEs) involve liquids during fabrication as well. The wetting procedure in GPEs containing aprotic solvents (e.g. propylene carbonate, ethylene carbonate)[62] might, therefore, not only be represented by a close distance between the surface of the Li metal and the electrolyte, but rather be accompanied by a squeezing effect of the solvent into the defects which would result in a phase separation and lead to much more complex wetting behaviors. We would like to stress that such wetting and phase separation phenomena at microscale and nanoscale should be verified for GPE-based systems as well and could lead to advanced electrolyte (as well as for the presented TSPEs) designs where improved wetting can be tailored by exploiting such mechanism.

Conclusion

In summary, we revealed that the morphological inhomogeneity of Li metal electrodes can have a significant influence on the electrochemical performance of such electrodes when cross-linked **SPE** and **TSPE** are present. Therefore, the roughness, not only of SEs, but also of the Li metal surface is critical.[63] The roughness will be further increased by pit/void formation during electrodeposition/electrodissolution. Such increased surface roughness is modelled in this work. The intentionally reshaped Li metal electrodes with V-shaped defects on the microscale can be considered as representative structures of lower surface area deposits (e.g. columnar Li deposits). We concluded in this work that the wetting behaviors as well as the mechanical properties of cross-linked PEO-based electrolytes have to be considered as key parameters and should not be overlooked when interfacial/interphasial properties are discussed. The overview of our conclusions is presented in Figure 5e. It is found that aside from the interfacial/interphasial resistances, the control of the "soft solid"–solid contact and the influence of surface curvatures on it is an often ignored but crucial factor at the Li | PE interface affecting Li electrodeposition/electrodissolution. Moreover, the diffusion properties at the interface are found to be dependent not only on the type of PE but also on the surface curvature. This was strongly pronounced for the **TSPE**, which tends to show a complex wetting behavior including a partial phase separation of the IL. In particular, the topography of defects deriving from formed pits/voids during cycling and inhomogeneous Li metal surface generated during production would lead to multiple behaviors of Li electrodeposition/electrodissolution, thus increasing difficulties to control the uniformity of Li deposits in solid-state

LMBs. Here we give a thought-provoking impulse that the wettability of PEs on the inevitably uneven Li metal surface needs deeper understanding (e.g. at nanoscale and study of contact mechanics under stacking pressure) and sophisticated design approaches are required to make PEs compatible and robust with varying Li surface topographies and enhance the stable and consistent long-term cycling performance of LMBs.

Acknowledgements

Financial support provided by the German Federal Ministry of Education and Research (BMBF) within MEET Hi-EnD II (03XP0084A; M.W., J.B.), MeLuBatt (03XP0110C; M.W., P.B., M.Z.), MgMeAnS (03XP0140; M.W., M.K.), and ProLiFest (03XP0253A; M.W., M.C.S.) is gratefully acknowledged. Furthermore, we thank the Friedrich Hahne – technische Schneidartikel e.K. company for supplying free samples of industrial blades. Special thanks to Philipp Schröder from the research group of Prof. Schönhoff (University of Münster) for time and support in rheological measurements, as well as Debbie Berghus (University of Münster) for DSC measurements. M.Z. wishes to thank Stefan van Bergerem (University of Münster) for preparation of membranes and impedance measurements and Xue-Qiang Zhang from Qiang Zhang's group (Tsinghua University) for discussions. Open access funding enabled and organized by Projekt DEAL.

Conflict of interest

The authors declare no conflict of interest.

Keywords: electrolyte wetting · lithium · nucleation · polymers · surface topography

[1] M. Winter, B. Barnett, K. Xu, *Chem. Rev.* **2018**, *118*, 11433 – 11456.
[2] T. Placke, R. Kloepsch, S. Dühnen, M. Winter, *J. Solid State Electrochem.* **2017**, *21*, 1939 – 1964.
[3] R. Schmuch, R. Wagner, G. Hörpel, T. Placke, M. Winter, *Nat. Energy* **2018**, *3*, 267 – 278.
[4] J. Liu, Z. Bao, Y. Cui, E. J. Dufek, J. B. Goodenough, P. Khalifah, Q. Li, B. Y. Liaw, P. Liu, A. Manthiram, et al., *Nat. Energy* **2019**, *4*, 180 – 186.
[5] Y. Zhang, T.-T. Zuo, J. Popovic, K. Lim, Y.-X. Yin, J. Maier, Y.-G. Guo, *Mater. Today* **2020**, *33*, 56 – 74.
[6] E. Peled, *J. Electrochem. Soc.* **1979**, *126*, 2047 – 2051.
[7] E. Peled, D. Golodnitsky, G. Ardel, V. Eshkenazy, *Electrochim. Acta* **1995**, *40*, 2197 – 2204.
[8] E. Peled, S. Menkin, *J. Electrochem. Soc.* **2017**, *164*, A1703 – A1719.
[9] G. Bieker, M. Winter, P. Bieker, *Phys. Chem. Chem. Phys.* **2015**, *17*, 8670 – 8679.
[10] M. He, R. Guo, G. M. Hobold, H. Gao, B. M. Gallant, *Proc. Natl. Acad. Sci. USA* **2020**, *117*, 73 – 79.
[11] X. Zhang, T. Li, B. Li, R. Zhang, P. Shi, C. Yan, J. Huang, Q. Zhang, *Angew. Chem. Int. Ed.* **2020**, *59*, 3252 – 3257; *Angew. Chem.* **2020**, *132*, 3278 – 3283.
[12] M. Winter, *Z. Phys. Chem.* **2009**, *223*, 1395 – 1406.
[13] V. Küpers, M. Kolek, P. Bieker, M. Winter, G. Brunklaus, *Phys. Chem. Chem. Phys.* **2019**, *21*, 26084 – 26094.
[14] M. H. Ryou, Y. M. Lee, Y. Lee, M. Winter, P. Bieker, *Adv. Funct. Mater.* **2015**, *25*, 834 – 841.
[15] X. B. Cheng, R. Zhang, C. Z. Zhao, Q. Zhang, *Chem. Rev.* **2017**, *117*, 10403 – 10473.
[16] S. Xia, X. Wu, Z. Zhang, Y. Cui, W. Liu, *Chem* **2019**, *5*, 753 – 785.
[17] W. Xu, J. Wang, F. Ding, X. Chen, E. Nasybulin, Y. Zhang, J.-G. Zhang, *Energy Environ. Sci.* **2014**, *7*, 513 – 537.
[18] A. Mauger, M. Armand, C. M. Julien, K. Zaghib, *J. Power Sources* **2017**, *353*, 333 – 342.
[19] J. Lopez, D. G. Mackanic, Y. Cui, Z. Bao, *Nat. Rev. Mater.* **2019**, *4*, 312 – 330.
[20] J. Janek, W. G. Zeier, *Nat. Energy* **2016**, *1*, 16141.
[21] H. Zhang, C. Li, M. Piszcz, E. Coya, T. Rojo, L. M. Rodriguez-Martinez, M. Armand, Z. Zhou, *Chem. Soc. Rev.* **2017**, *46*, 797 – 815.
[22] E. Quartarone, P. Mustarelli, *Chem. Soc. Rev.* **2011**, *40*, 2525 – 2540.
[23] A. Mauger, C. M. Julien, J. B. Goodenough, K. Zaghib, *J. Electrochem. Soc.* **2020**, *167*, 070507.
[24] J. R. Nair, L. Imholt, G. Brunklaus, M. Winter, *Electrochem. Soc. Interface* **2019**, *28*, 55 – 61.
[25] P. Hovington, M. Lagacé, A. Guerfi, P. Bouchard, A. Mauger, C. M. Julien, M. Armand, K. Zaghib, *Nano Lett.* **2015**, *15*, 2671 – 2678.
[26] B. Rupp, M. Schmuck, A. Balducci, M. Winter, W. Kern, *Eur. Polym. J.* **2008**, *44*, 2986 – 2990.
[27] M. Falco, C. Simari, C. Ferrara, J. R. Nair, G. Meligrana, F. Bella, I. Nicotera, P. Mustarelli, M. Winter, C. Gerbaldi, *Langmuir* **2019**, *35*, 8210 – 8219.
[28] M. Wetjen, G. T. Kim, M. Joost, M. Winter, S. Passerini, *Electrochim. Acta* **2013**, *87*, 779 – 787.
[29] H. Liu, X. Cheng, R. Xu, X. Zhang, C. Yan, J. Huang, Q. Zhang, *Adv. Energy Mater.* **2019**, *9*, 1902254.
[30] J. Park, J. Jeong, Y. Lee, M. Oh, M. H. Ryou, Y. M. Lee, *Adv. Mater. Interfaces* **2016**, *3*, 1600140.
[31] Y. J. Kim, H. S. Jin, D. H. Lee, J. Choi, W. Jo, H. Noh, J. Lee, H. Chu, H. Kwack, F. Ye, et al., *ChemElectroChem* **2018**, *5*, 3169 – 3175.
[32] J. Kasemchainan, S. Zekoll, D. Spencer Jolly, Z. Ning, G. O. Hartley, J. Marrow, P. G. Bruce, *Nat. Mater.* **2019**, *18*, 1105 – 1111.
[33] T. Krauskopf, H. Hartmann, W. G. Zeier, J. Janek, *ACS Appl. Mater. Interfaces* **2019**, *11*, 14463 – 14477.
[34] J. Kasnatscheew, R. Wagner, M. Winter, I. Cekic-Laskovic, *Top. Curr. Chem.* **2018**, *376*, 16.
[35] C. Xu, B. Sun, T. Gustafsson, K. Edström, D. Brandell, M. Hahlin, *J. Mater. Chem. A* **2014**, *2*, 7256 – 7264.
[36] Q. Ma, X. X. Zeng, J. Yue, Y. X. Yin, T. T. Zuo, J. Y. Liang, Q. Deng, X. W. Wu, Y.-G. Guo, *Adv. Energy Mater.* **2019**, *9*, 1 – 7.
[37] S. Choi, M. Jeon, W. D. Jung, S. Yang, S. Park, H.-I. Ji, J.-H. Lee, B.-K. Kim, B.-I. Sang, H. Kim, *Solid State Ionics* **2020**, *346*, 115217.
[38] J. Becking, A. Gröbmeyer, M. Kolek, U. Rodehorst, S. Schulze, M. Winter, P. Bieker, M. C. Stan, *Adv. Mater. Interfaces* **2017**, *4*, 1700166.
[39] M. Zhang, A. L. Gui, W. Sun, J. Becking, O. Riedel, X. He, D. Berghus, V. Siozios, D. Zhou, T. Placke, et al., *J. Electrochem. Soc.* **2019**, *166*, A2142 – A2150.
[40] L. Frenck, J. A. Maslyn, W. S. Loo, D. Y. Parkinson, N. P. Balsara, *ACS Appl. Mater. Interfaces* **2019**, *11*, 47878 – 47885.
[41] D. Liebenau, K. Jalkanen, S. Schmohl, M. C. Stan, P. Bieker, H. D. Wiemhöfer, M. Winter, M. Kolek, *Adv. Mater. Interfaces* **2019**, *6*, 1900518.
[42] F. Li, J. Li, F. Zhu, T. Liu, B. Xu, T.-H. Kim, M. J. Kramer, C. Ma, L. Zhou, C.-W. Nan, *Matter* **2019**, *1*, 1001 – 1016.

[43] Y. Zhang, Y. Shi, X. Hu, W. Wang, R. Wen, S. Xin, Y.-G. Guo, *Adv. Energy Mater.* **2020**, *10*, 1903325.
[44] G. T. Kim, G. B. Appetecchi, M. Carewska, M. Joost, A. Balducci, M. Winter, S. Passerini, *J. Power Sources* **2010**, *195*, 6130 – 6137.
[45] H. Lin, E. Van Wagner, J. S. Swinnea, B. D. Freeman, S. J. Pas, A. J. Hill, S. Kalakkunnath, D. S. Kalika, *J. Membr. Sci.* **2006**, *276*, 145 – 161.
[46] Y. Gu, J. Zhao, J. A. Johnson, *Angew. Chem. Int. Ed.* **2020**, *59*, 5022 – 5049; *Angew. Chem.* **2020**, *132*, 5054 – 5085.
[47] M. Eftekharnia, M. Hasanpoor, M. Forsyth, R. Kerr, P. C. Howlett, *ACS Appl. Energy Mater.* **2019**, *2*, 6655 – 6663.
[48] R. Inada, S. Yasuda, H. Hosokawa, M. Saito, T. Tojo, Y. Sakurai, *Batteries* **2018**, *4*, 26.
[49] M. Rosso, T. Gobron, C. Brissot, J. N. Chazalviel, S. Lascaud, *J. Power Sources* **2001**, *97 – 98*, 804 – 806.
[50] A. Pei, G. Zheng, F. Shi, Y. Li, Y. Cui, *Nano Lett.* **2017**, *17*, 1132 – 1139.
[51] M. D. Berliner, B. C. McGill, M. Majeed, D. T. Hallinan, *J. Electrochem. Soc.* **2019**, *166*, A297 – A304.
[52] X. Guan, A. Wang, S. Liu, G. Li, F. Liang, Y.-W. Yang, X. Liu, J. Luo, *Small* **2018**, *14*, 1801423.
[53] P. G. Bruce, C. A. Vincent, *J. Electroanal. Chem.* **1987**, *225*, 1 – 17.
[54] D. M. Pesko, Z. Feng, S. Sawhney, J. Newman, V. Srinivasan, N. P. Balsara, *J. Electrochem. Soc.* **2018**, *165*, A3186 – A3194.
[55] F. Single, B. Horstmann, A. Latz, *J. Phys. Chem. C* **2019**, *123*, 27327 – 27343.
[56] E. Warburg, *Ann. Phys. Chem.* **1899**, *303*, 493 – 499.
[57] J. Huang, *Electrochim. Acta* **2018**, *281*, 170 – 188.
[58] J. E. B. Randles, *Discuss. Faraday Soc.* **1947**, *1*, 11 – 19.
[59] X. Huang, L. Chen, J. Schoonman, *J. Power Sources* **1993**, *44*, 487 – 492.
[60] K.-H. Chen, K. N. Wood, E. Kazyak, W. S. LePage, A. L. Davis, A. J. Sanchez, N. P. Dasgupta, *J. Mater. Chem. A* **2017**, *5*, 11671 – 11681.
[61] S. A. Pervez, G. Kim, B. P. Vinayan, M. A. Cambaz, M. Kuenzel, M. Hekmatfar, M. Fichtner, S. Passerini, *Small* **2020**, *16*, 2000279.
[62] D. Zhou, D. Shanmukaraj, A. Tkacheva, M. Armand, G. Wang, *Chem* **2019**, *5*, 2326 – 2352.
[63] K. K. Fu, Y. Gong, B. Liu, Y. Zhu, S. Xu, Y. Yao, W. Luo, C. Wang, S. D. Lacey, J. Dai, et al., *Sci. Adv.* **2017**, *3*, e1601659.

Manuscript received: February 4, 2020
Accepted manuscript online: June 15, 2020
Version of record online: August 4, 2020

